Study of Plasma-Polyethylene Interactions Using Electron Beam-Generated Plasmas Produced in Ar/SF_6 Mixtures

S. G. Walton,[1] E. H. Lock,[1] A. Ni,[1,2] M. Baraket,[1,2] R. F. Fernsler,[1] D. D. Pappas,[3] K. E. Strawhecker,[3] A. A. Bujanda[3]

[1]*Plasma Physics Division, U.S. Naval Research Laboratory, Washington, District of Columbia 20375*
[2]*Global Strategies, Inc., Crofton, Maryland 21114*
[3]*Army Research Laboratory, Aberdeen Proving Ground, Maryland 21005*

Received 20 November 2009; accepted 5 February 2010
DOI 10.1002/app.32249
Published online 12 May 2010 in Wiley InterScience (www.interscience.wiley.com).

ABSTRACT: The use of electron beam-generated plasmas produced in Ar/SF_6 mixtures to modify the surface of ultra-high molecular weight polyethylene substrates is discussed. Changes in the surface energy, chemistry, and morphology are presented as a function of plasma operating parameters, along with simple system diagnostics to obtain a better understanding of the plasma-polymer interaction. For all conditions, the hydrophobicity of the material was increased via the incorporation of fluorine, and for some conditions, the surface was found to remain stable over the course of 1 year. © 2010 Wiley Periodicals, Inc.† J Appl Polym Sci 117: 3515–3523, 2010

Key words: aging; functionalization of polymers; fluorination; polyethylene; cold plasma

INTRODUCTION

Polymers are widely used in the production of new materials and devices ranging from biomaterials[1] to organic[2] and flexible[3] electronics. Although the bulk characteristics of polymers are attractive for these and other applications, their surface characteristics are often not well-suited for the given application and must be altered before use. Plasma-based techniques are particularly good for altering the surface characteristics without affecting the bulk properties and have a number of advantages over other techniques, including low pollution and waste products, uniform treatment over surface features, and room-temperature processing. Plasma-produced energetic ions and reactive species are known to produce chemically active sites on the polymer surface that can lead to the desired functionality. Indeed, plasmas have been used to improve adhesion,[4] wettability,[5] hydrophobicity,[5] and biocompatibility.[6]

Ultra-high molecular weight polyethylene (UHMWPE) is a common polymer used in biomaterials,[7] composite applications,[8] and in the production of synthetic fibers.[9] The hydrophobicity of UHMWPE will directly influence performance. Hydrophobic materials prevent bacterial growth in prosthetic devices, provide increased scratch resistance in optical coatings, and are used in various packaging and nonsticking applications.[10] Hydrophobicity is often enhanced by increasing the fluorine concentration at the surface. In plasma processing, this is typically accomplished by treating the surface with plasmas produced in a fluorine containing gas (F, SF_6, C_3F_6, etc.). The level of hydrophobicity will, however, depend not only on the F concentration but also on the amount of oxygen present as well as the surface morphology. For long term stability, it is important that the ratio of fluorine to oxygen does not increase after treatment. The hydrophobic characteristics of polyethylene terephthalate treated with a sulfur hexafluoride (SF_6) discharge was found to depend on the operating parameters of the plasma.[11] The competing processes of surface etching, which leads to radical activation and oxidation, and fluorine grafting were identified as the most likely reasons that the relative hydrophobicity varied. More specifically, if ion-assisted etching could be reduced by reducing the kinetic energy of ions incident to the surface, the incorporation of F could be maximized, thereby enhancing the hydrophobic character of the surface.

The Naval Research Laboratory has developed a material processing system based on electron beam-generated plasmas for use in a range of applications.[12,13] When high-energy ($\approx$ 2 keV) electron beams are used as the primary ionization source, the

Correspondence to: S. G. Walton (scott.walton@nrl.navy.mil).

Contract grant sponsor: Office of Naval Research and the Army Research Laboratory and National Research Council.

resultant plasmas have several unique characteristics when compared with conventional low-pressure plasma sources. Plasma production is confined to the electron beam volume, and so chamber and source geometry can be readily modified to suit the processing application. Moreover, the ion flux at the substrate surface can be regulated by moving the substrate position with respect to the electron beam.[14] Also, unlike other plasma sources, species production rates are nearly directly proportional to the background gas concentrations[14] and can thus be easily adjusted; the total production rate can be changed by varying the beam current density.[15] Lastly and importantly for this work, the plasma electron temperature is inherently low, which provides a low plasma potential, and thus, low ion energy as they leave the plasma.[16] In molecular gases, those energies are typically below 3 eV.[14]

This inherently low incident ion energy provides a unique opportunity to study polymer modification as the kinetic energies are close to the binding energies of the species that make up the polymer chains and etching is minimized. Electron beam-generated plasmas have already been used to change the functionality and surface chemistry of polymers,[4] whereas it was also shown that these plasmas have less impact on the surface roughness in polymers[17,18] than treatments by conventional discharges.[19] In previous work,[20] these plasmas, produced in mixtures containing SF_6, were used to modify the surfaces of solid and porous polyethylene, demonstrating an increase in hydrophobicity. We also demonstrated the impact of grafted oxygen groups via dielectric barrier discharge on the surface wettability.[21] In this work, we focus on the modification of solid, UHMWPE using electron beam-generated plasmas produced in background containing very small concentrations of SF_6. We discuss changes in the surface energy, chemical composition, and roughness as a function of operating parameters. We also include simple system diagnostics, and the results are correlated to the observed changes in the polymer surface. Most importantly, we demonstrate that the plasma-induced surface hydrophobicity is because of the grafting of fluorine functionalities making this process a promising, lightweight alternative to teflon-like deposited coatings.

EXPERIMENTAL

Processing system and diagnostics

The production of electron beam-generated plasmas has been described in detail elsewhere.[22] The experimental apparatus is shown in Figure 1 and includes a simplified circuit diagram used for system diagnostics. The system vacuum was maintained by a

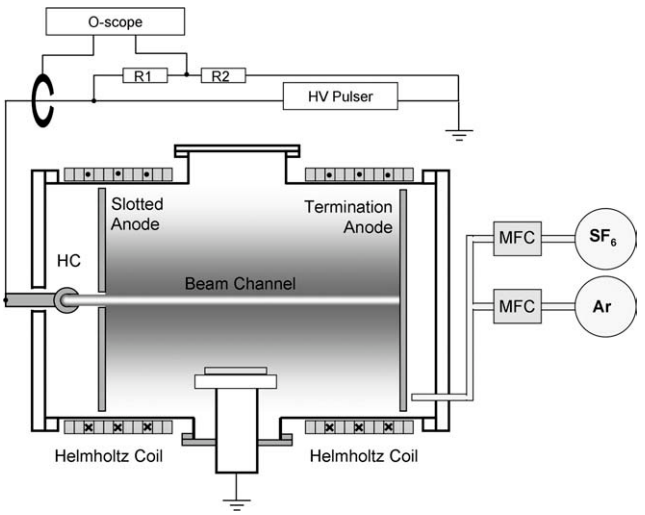

Figure 1 Diagram of the plasma processing system and related circuit used to measure cathode voltage and current.

250 l/s turbo pump, with a base pressure in the order of 10^{-7} Torr. The operating pressure (25–75 mTorr) was achieved by introducing high-purity gases through mass flow controllers and throttling the pumping speed using a manual gate valve. In all cases, the total flow was fixed at 50 sccm and the SF_6 flow was varied between 0.5 and 2.5 sccm. A set of external field coils provided an axial magnetic field of 150 Gauss that varied by no more than 5% over the region of interest.

Plasmas were generated by high-energy electron beams produced by driving the hollow cathode with a -2 kV pulse for a duration of 1–4 ms at a duty factor of 5–40%. The emergent beam passed through a slot in a grounded anode and was then terminated at a second grounded anode located farther downstream. The electron beam volume between the two anodes defines the ionization source volume, with the dimensions set by the slot size (1 cm $\times$ 20 cm) and the anode-to-anode length (40 cm).

It is important to note that pulsing the hollow cathode produces an electrical discharge between the negatively biased cathode and the grounded, slotted anode. The discharge is sustained by gas ionization and secondary emission at the cathode, but the beam is composed primarily of secondary electrons, emitted from the back surface of the cathode; secondary electrons emitted from the side walls are assumed to be reflected by the cathode sheath, producing the hollow cathode effect.[23] Although the actual beam current is not known, it is assumed to be about 10–20% of the discharge current, based on the secondary electron emission coefficient. The voltage pulse is monitored by reading the voltage across a voltage divider, whereas the discharge current is

TABLE I
Table of Standard Operating Conditions Use in This Work

Parameter	Value
Total Pressure	50 mTorr
Ar flow	47.5 sccm
SF_6 flow	2.5 sccm
Period	20 ms
Pulse width	2 ms
Duty	10%
Treatment time	12 s

measured using a current transformer (Ion Physics Corp. model #CM-1-L).

Surface treatment and diagnostics

The material used in this work consisted of thin (75 μm), solid UHMWPE films (Goodfellow). The samples were placed on an electrode located ~ 2.5 cm from the center of the beam. Before each treatment, the chamber was evacuated to a base pressure of 2–4 × 10^{-6} Torr. After treatment, the chamber was again evacuated to base pressure for 5 min before venting the system and removing the materials for ex situ surface diagnostics. A number of operating conditions were explored, including variations in the period and pulse width (duty factor), total pressure, relative gas concentrations, and treatment time. When exploring operating conditions, only one was varied while the rest were held fixed at arbitrarily chosen "standard" conditions. For this work, those conditions (see Table I) include: P = 50 mTorr, Ar flow = 47.5 sccm, SF_6 flow = 2.5 sccm, Period = 20 ms, PW = 2 ms, 12 s exposure. We have defined "treatment time" as the total time the plasma is on (i.e., operation time multiplied by the duty factor). This description is based on the presumption that the electron beam is solely responsible for the production of ions and radicals in the gas.

Post-treatment surface diagnostics included X-ray photoelectron spectroscopy (XPS), atomic force microscopy (AFM), and goinometry to determine the chemical composition, surface morphology, and surface energy, respectively. Near surface compositional depth profiling was performed using the Kratos Axis Ultra 165 XPS system, equipped with a hemispherical analyzer. A 100 W monochromatic A1 Ka (1486.7 eV) beam irradiated a 1 mm × 0.5 mm sampling area with a take-off angle of 90°. The pressure in the XPS chamber was held between 10^{-9} and 10^{-10} Torr. Elemental high resolution scans for C1s, O1s, nd F1s, were taken at the pass energy of 20 eV. A value of 285.0 eV for the hydrocarbon C1s core level was used as the calibration energy for the binding energy scale. Several areas on each sample were analyzed to test the uniformity of the treatment.

The contact angle measurements were performed on automatic VCA (AST Products). Water, diiodomethane, and ethylene glycol were chosen as liquids with known surface energies. The volume of the drops (2 μL) was kept constant. The Owens–Wendt model[24] was used to estimate the surface energy of the polymer surface.

AFM was performed using a Dimension 3100 microscope with a Nanoscope IV controller (Digital Instruments/Veeco). Imaging was done in tapping mode, using TESP (silicon) cantilevers (Veeco Probes) at nominally 0.5 Hz scan rate and "moderate" tapping force setpoints (~ 60–75% of the free-air oscillation amplitude.) Scan ranges were 50 microns laterally (x and y). Using Nanoscope software (v6.13r1), images were 1st order x–y plane fitted and then 1st order flattened, followed by roughness analysis. Root mean square (RMS) roughness values from 4 to 6 images, obtained from different locations on each sample, were averaged; outliers (high and low from each dataset) were discarded in the reported average and standard deviations.

RESULTS AND DISCUSSION

Figures 2–5 show the change in surface chemistry, energy, and roughness as operating parameters were varied. For all figures, the zero of the abscissa

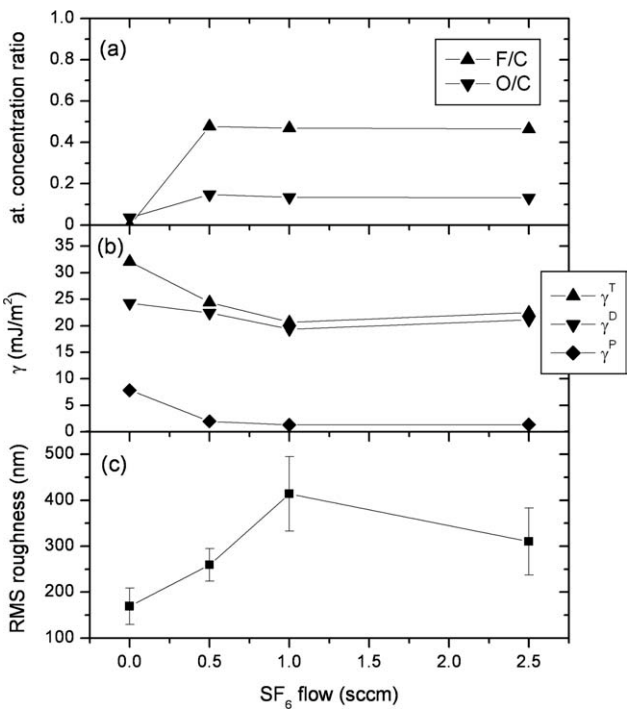

Figure 2 Surface characteristics as a function of the SF_6 flow. The zero of the abscissa refers to the untreated sample. (a) Ratio of fluorine-to-carbon and oxygen-to-carbon; (b) The total (γ^T), dispersive(γ^d), and polar (γ^P) components of surface energy; (c) The RMS surface roughness.

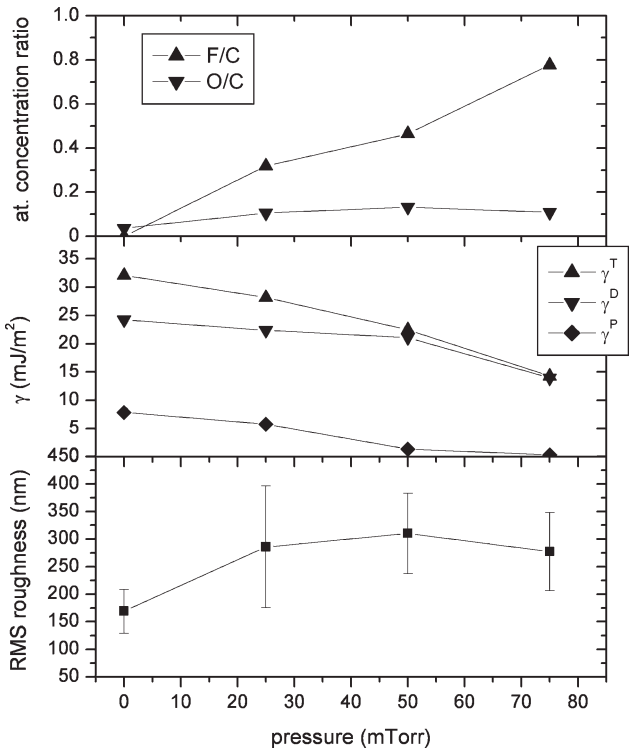

Figure 3 Surface characteristics as a function of the total operating pressure. The zero of the abscissa refers to the untreated sample.

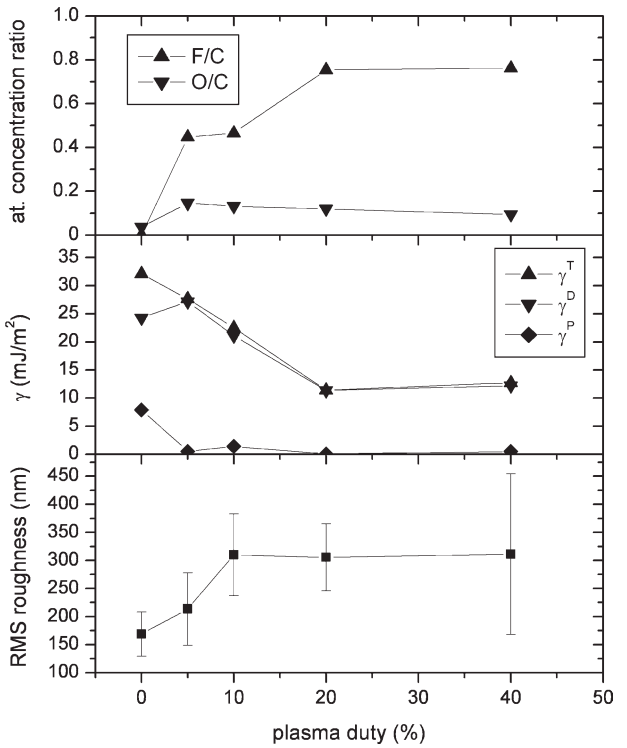

Figure 4 Surface characteristics as a function of the plasma duty factor (pulse width/period). The zero of the abscissa refers to the untreated sample.

represents the values for the as-received (untreated) films. The results of Figures 2–5 are summarized in Figure 6 where the chemistry, energy, and roughness change are plotted as a function of the range of operating conditions. Here, zero is the value before the plasma exposure and one is the highest value in the range of operating conditions (i.e., one corresponds to 2.5 sccm, 75 mTorr, 40% duty, and 60 s exposure). The results of Figure 6 show that a range of values are achievable, depending on the operating conditions. Specifically, the atomic fluorine concentration ranged between about 12 and 40%, surface energy was decreased between 15 and 50%, and RMS roughness varied between about 210 and 480 nm after treatment, compared with approximately 170 nm for the untreated sample. For all process parameters, with the exception of pressure, the surface conditions generally saturate with an increase in operating parameters. In the case of pressure, a slower increase (or decrease) is observed. We will address the specifics of each measured surface characteristic in the following sections.

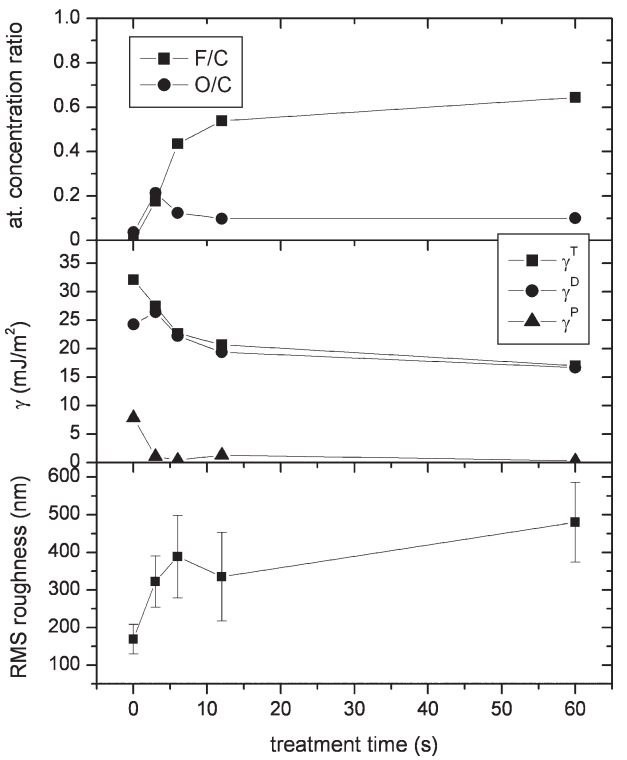

Figure 5 Surface characteristics as a function of the treatment time. Treatment time is defined as the plasma exposure time. The zero of the abscissa refers to the untreated sample.

Surface chemistry

Figure 7 presents the XPS survey spectrum of a polyethylene film treated in Ar/SF_6 for 60 s. The spectrum for the as-received polyethylene (inset) consists of a single peak located at 285 eV, which

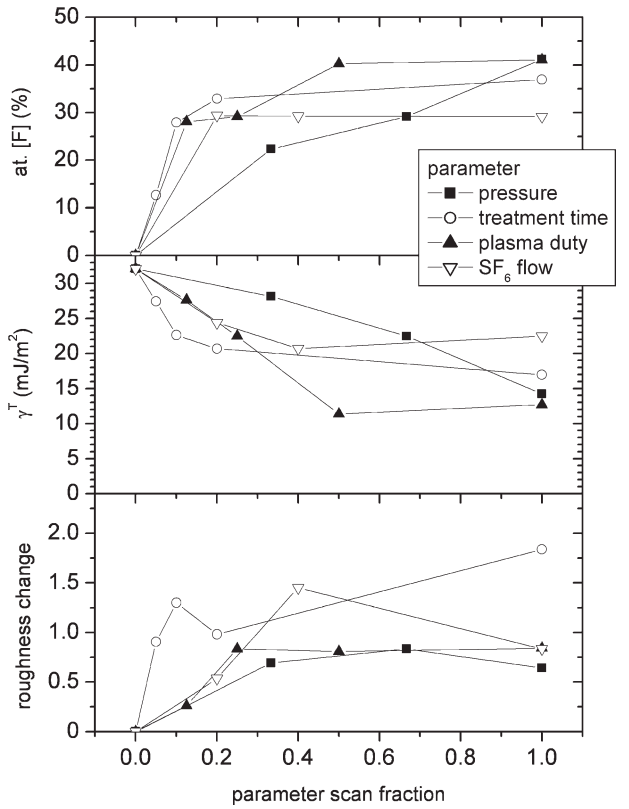

Figure 6 Surface characteristics as a function of the fraction of the parameter ranges presented in Figures 2–5. In (b), only the total surface energy is plotted and in (c), the relative increase in roughness, compared to the untreated material, is plotted. The zero of the abscissa refers to the untreated sample.

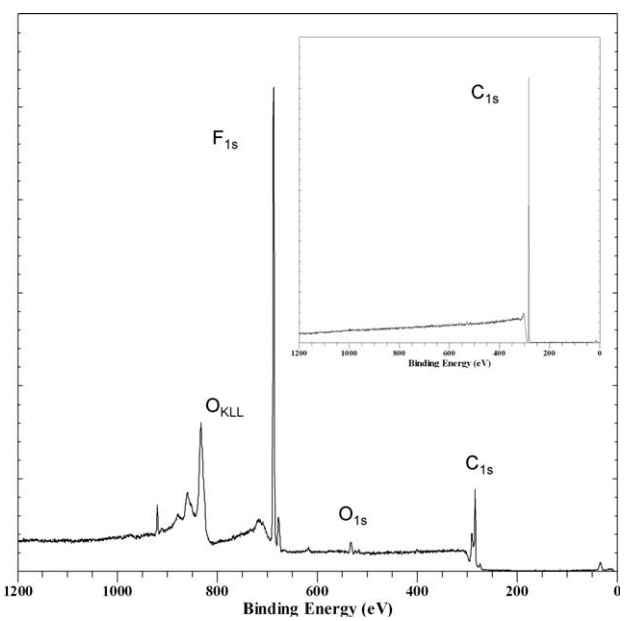

Figure 7 XPS survey spectrum of UHMWPE processed at standard operating conditions (see Table I). (Inset) XPS survey spectrum of as-received UHMWPE.

can be identified as C1s, and the survey spectrum for the plasma-treated surface shows the presence of oxygen (O1s, 530 eV) and an intense fluorine peak (F1s, 685 eV). The calculated atomic concentrations of F, O, and C for the plasma treated film were 45.32, 2.31, and 51.38%, respectively. As seen in Figures 2(a)–4(a) the plasma processing parameters have an impact on the surface fluorine atomic concentration. In all cases, fluorine uptake is observed, although the variations are dependent on the specific parameters. Most importantly, limited oxygen uptake is observed in all samples studied. The formation of F—O bonds is thermodynamically unfavorable[25] and so, the limited oxygen uptake is likely through the formation of carbon-oxygen functionalities after plasma treatment. As seen in Figure 6 the saturation of the surfaces occurs within 10 s of plasma exposure and more prolonged treatments do not increase fluorine content significantly.

Figure 8 shows high-resolution XPS analysis of plasma-treated and as-received UHMWPE films. The C1s spectrum of the untreated film (Fig. 8 inset) shows a narrow hydrocarbon peak located at 285 eV. The spectrum of the plasma-treated samples shows the existence of the plasma-induced fluorine-containing species, attributed to different CH—F_x and fluorine-related carbon species. Deconvolution of the C1s peak was performed using the following components: C—C, C—H at 285.0 eV, C—CF_n and/or C—O, C—OH at 286.7 eV, CF at 289.1 eV, CF_2 at 291.2 eV and CF_3 at 293.1 eV.[26] Comparison of the

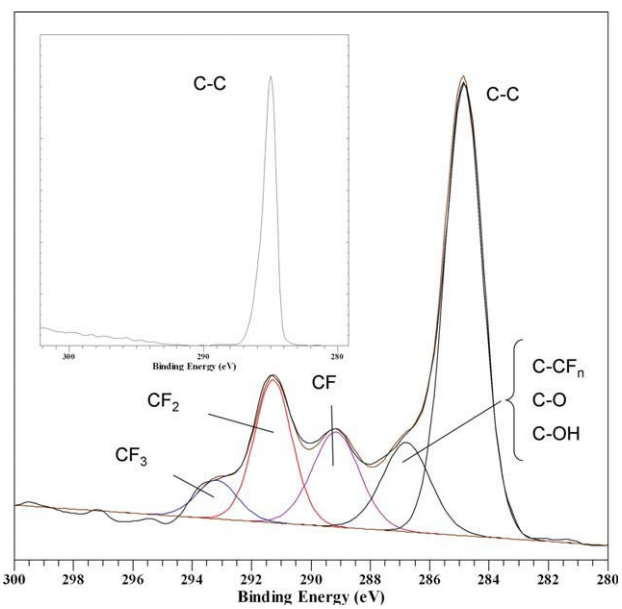

Figure 8 High-resolution XPS spectrum of the C1s peak of UHMWPE processed at standard operating conditions (see Table I). (Inset) As-received UHMWPE high-resolution XPS spectrum of the C1s peak. [Color figure can be viewed in the online issue, which is available at www.interscience.wiley.com.]

two high-resolution spectra, for the as-received and plasma treated polyethylene, show a significant decrease of the C—C, C—H peaks after the plasma exposure that can be attributed to chain scission or crosslinking because of the bombardment of the plasma energetic species on the polymer surface. Furthermore, the delivery of fluorine to the surface provides a channel for hydrogen elimination via the formation of volatile hydrofluoric acid (HF). Fluorine, which has a higher electron affinity than hydrogen, can then be added to the dangling bonds created by hydrogen abstraction.[27] Based on extended Huckel molecular orbital calculations, the attachment of fluorine atoms to free radical sites does not cause significant disturbance of the adjacent C—C σ bond,[28] and thus, it gives rise to the saturated bonding configuration.

It is also important to note that no change in the surface chemistry was observed after washing the surface with deionized water. That is, XPS results before and after washing are identical, thus indicating fluorine is covalently bound to the polymer backbone, rather than simply chemisorbed on the surface. This is also an indication that there are no low molecular weight fragments present on the surface that would be removed with rinsing.

Surface energy

For all studied parameters (SF_6 flow [Fig. 2(b)], pressure [Fig. 3(b)], duty factor [Fig. 4(b)], and treatment time [Fig. 5(b)]), a decrease in the surface energy was observed. In all cases, the polar component of the surface energy is reduced to near zero so that surface energy is described almost solely by its dispersive (or apolar) component. The lowest surface energy occurs at the largest pressure and highest duty factor; the surface energies of the fluorinated surfaces at 40% duty factor and at 75 mTorr are approximately half of their original value (≈ 32 mJ/m^2). The surface energy is lowest at the longest treatment time and lower yet at the largest SF_6 flow. As a function of treatment time, only small changes in surface energy were observed after 6 s of treatment. Similarly, only small changes in surface energy were observed as the SF_6 flow was varied. On the other hand, changes in duty and pressure produced the largest variation, indicating these two variables have a greater influence. As will be discussed later, the importance of duty factor and operating pressure is related to the production of reactive species.

An important consideration in surface modification is not only the final values after treatment but also the stability of the surface with time, and so aging experiments were performed. For these studies, no effort was made to regulate the environment in which the samples were stored. Between measurements, the samples were held under ambient laboratory conditions, with a cover to avoid dust accumulation. Figure 9 shows the change in surface energy of samples processed for various times, while keeping all other variables fixed at the standard conditions. The surface energy was tracked over the course of about 1 year and the observed hydrophilic recovery was dependent on treatment time. For the shortest treatment time (3 s), the surface energy returned to its original value. For intermediate times the recovery was about 20% but not complete. The recovery of oxygenated polymers after plasma treatment is well documented and is caused by migration of polar oxygen functionalities from the surface of the polymer toward the bulk.[18,29,30] For the longest treatment time, essentially no change in surface energy was observed. A number of mechanisms could be responsible for this. The formation of a crosslinked layer near the surface promoted by the dehydrogenation of polyethylene[31,32] or a flux of VUV photons.[33] It is also possible that surface stability is derived from fluorine saturation. That is, when hydrogen is replaced by fluorine, there are fewer sites available for oxygen incorporation, and thus, little chance for recovery. Note the relationship in Figure 5, between F/C and O/C and surface energy. These results are significant because they show that the treatment can produce surfaces with extended shelf lives, which is not characteristic for plasma-treated polymers. Stable, highly hydrophobic surfaces can act as barrier layers against solvent and fuel permeation.[34]

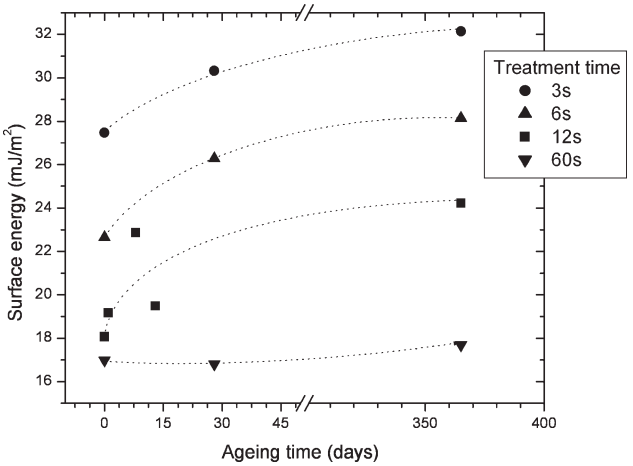

Figure 9 Aging studies of UHMWPE samples exposure for various treatment times. The zero of the abscissa indicates the surface energy immediately following plasma exposure. The dotted lines are meant to guide the eye.

Surface roughness

Shown in Figure 10 are images of untreated UHMWPE and a sample treated for 60 s, a

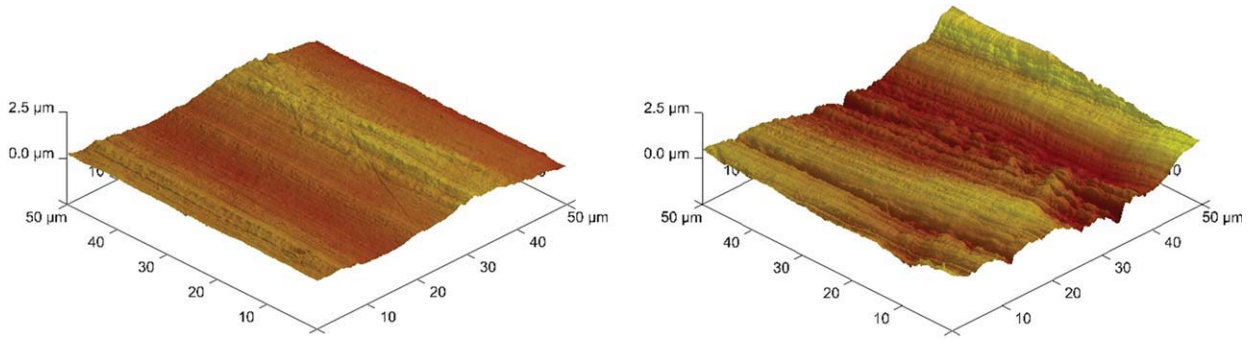

Figure 10 AFM images of UHMWPE samples. (Left) untreated and (right) a sample treated for 60 s. While all other conditions were standard (see table I). [Color figure can be viewed in the online issue, which is available at www.interscience.wiley.com.]

comparison of the two extremes in roughness. AFM analysis showed that the untreated polyethylene film surface had RMS roughness of about 170 nm with smooth hills and valleys being the predominant features. The RMS roughness of the treated sample was about 480 nm and the image reveals a general enhancement of roughness, along with a more pronounced difference between the hills and valleys.

System diagnostics

In electron beam-generated plasmas, it is the high-energy electrons from the beam and not the plasma electrons, which are the primary producer of species and so, with a few assumptions, it is possible to estimate the ion and neutral dose at the polymer surface. For this work, we focus on the fluorine dose. From (15), the ionization rate of SF_6 will be proportional to the beam current density, J_b, the SF_6 density, n_g, and the ionization cross section, σ_i. For these experiments, we can calculate the production rate of fluorine $S(F)$ from the primary ionization channel,

$$e^- + SF_6 \rightarrow SF_5^+ + F + 2e^-, \quad (1)$$

using the relationship,

$$S(F) = kD_f I_c P(f_{SF_6}/f_T)\sigma_i. \quad (2)$$

Here I_c is the cathode current, which is assumed to be proportional to the beam current, P is the total gas pressure, f_x is the gas flow, which is assumed to be proportional to the density of species x, D_f is the duty factor, and k is a constant.

Shown in Figures 11–13, are the measured cathode currents as a function of the parameters used in the processing along with the production rates calculated using eq. (2). To get smooth production rates through the parameter range and beyond, best fits of the measured currents were used. A linear fit was used for both the flow rate and operating pressure, whereas the best fit for duty factor was an exponential decay. Although the scale for production is arbitrary, the results were generated using the standard processing conditions and so the production rates in all graphs can be compared. Note here that only the dominant ionization reaction is considered and so the production of F via other mechanisms, such as other ionization channels and dissociative charge exchange, is not formally considered. Most, but not all of these other processes are absorbed by the dimensionless parameter k in eq. (1). The trends indicate that the production rates vary strongest with pressure, a reasonable result, given that both the gas density and cathode discharge current (providing a higher beam density) increase.

As most F atoms are assumed to come from this reaction, we may estimate the total dose at the polymer surface using,

$$D = S(F)t, \quad (3)$$

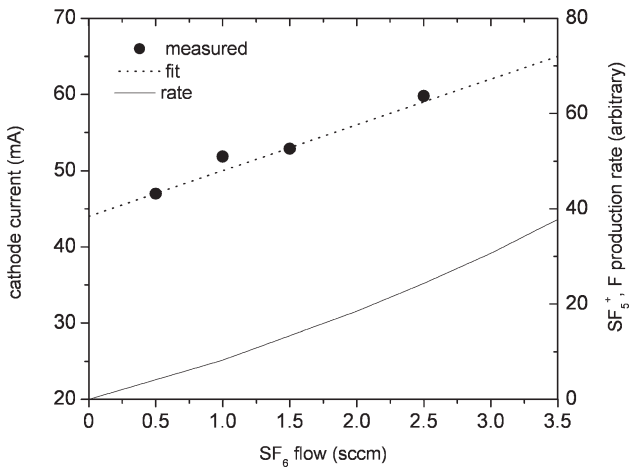

Figure 11 Cathode current measured as a function of SF_6 flow along with a linear fit. All other operating conditions were standard (see Table I). Also shown is the production rate of species in eq. (1), calculated using eq. (2).

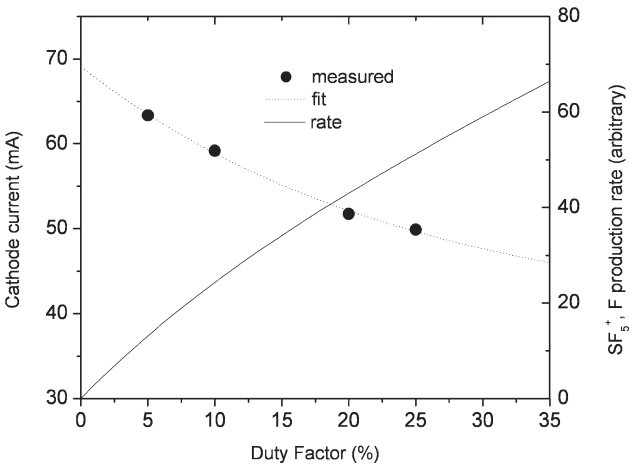

Figure 12 Cathode current measured as a function of plasma duty factor along with an exponential decay fit. All other operating conditions were standard (see Table I). Also shown is the production rate of species in eq. (1), calculated using eq. (2).

where t is the exposure time. The results of this calculation, using standard conditions, maximum duty factor and maximum pressure, are shown in Figure 14. Here, we assume that the only destruction mechanism for F is diffusion to the walls or through the pump. Clearly, the relative destruction rates will change as the sticking coefficient at the walls is coverage dependent and the pressure was varied by changing the pumping speed.

In Figure 14, the longest exposure time (60 s) resulted in the largest dose. However, for standard exposure times (12 s), the largest dose occurred at the maximum pressure (nearly equal to the value at the largest duty), whereas the lowest occurs at the maximum flow (indicated by the arrow on the standard conditions line). With the exception of the longest exposure time, the dose estimates correlate well with the processing results (Fig. 6). That is, the highest pressure and largest duty factor produces the largest incorporation of F in the polymer surface. It is assumed that the incorporation of F with long exposure times (>12 s) saturates because of the competing process of etching. Although we focused the discussion on fluorine dose, it should be noted that the longest exposure times result in the largest dose of ions as well, and it is not surprising that the largest RMS roughness occurs at the longest exposure times.

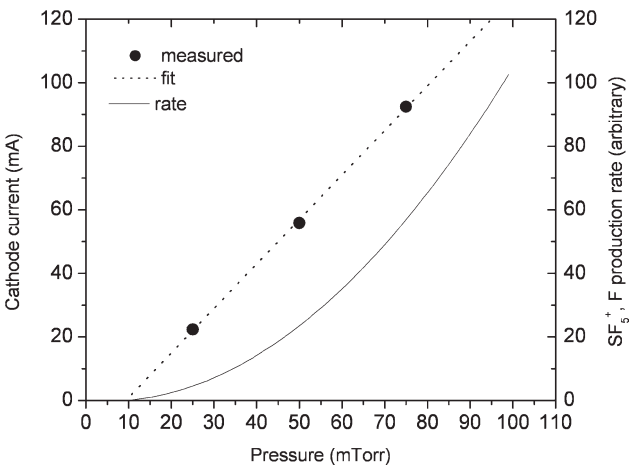

Figure 13 Cathode current measured as a function of operating pressure. All other operating conditions were standard (see Table I). Also shown is the production rate of species in eq. (1), calculated using eq. (2).

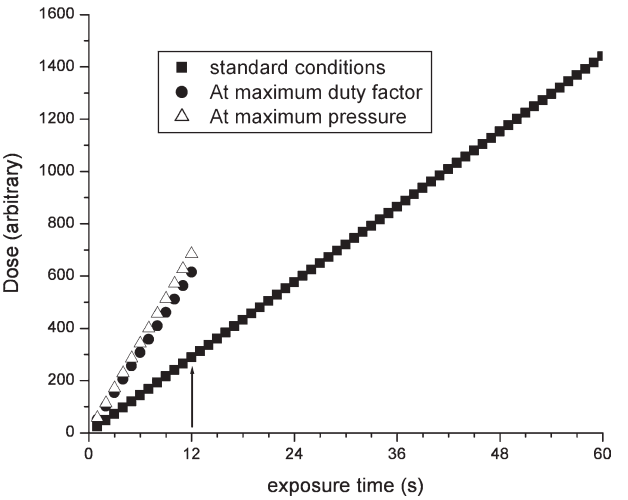

Figure 14 Fluorine dose at the polymer surface calculated using eq. (3) as a function of treatment time at maximum duty factor, pressure, and treatment time. The standard conditions (see Table I) curve shows both the true standard conditions (arrow at 12 s) the maximum exposure time (60 s).

SUMMARY

In this work, we used pulsed electron beam-generated plasma produced in Ar/SF_6 mixtures to functionalize the surface of UHMWPE. The relative amount of the fluorine incorporation was found to depend on the operating conditions of the system, as was the surface energy and roughness. The atomic fluorine concentration ranged between about 12 and 40%, and surface energy was decreased by between 15 and 50%. RMS roughness varied between about 210 and 480 nm after treatment, compared with roughly 170 nm for the untreated sample. Plasma diagnostics linked the increased surface fluorine, decrease in surface energy, and increase in roughness to the production of fluorine. Aging studies showed that stable surfaces could be obtained under some operating conditions, resulting in only small changes in surface energy over the course of 1 year. The results indicate an ability to regulate the surface

characteristics, thus producing hydrophobic surfaces that are extremely stable in time.

References

1. Simmel, F. C.; Dittmer, W. U. Small 2005, 1, 284.
2. Deen, M. J.; Kazemeini, M. H. Proc IEEE 2005, 93, 1306.
3. Tarighat, R. S.; Goodarzi, A.; Mohajerzadeh, S.; Arvan, B.; Gaderi, M. R.; Fathipour, M. Proc IEEE 2005, 93, 1374.
4. Leonhardt, D.; Muratore, C.; Walton, S. G. IEEE Trans Plasma Sci 2005, 33, 783.
5. Hegemann, D.; Brunner, H.; Oher, C. Nucl Instrum Methods Phys Res B 2003, 208, 281.
6. Garrison, M.; Luginbel, R.; Overney, R.; Ratner, B. Thin Solid Films 1999, 352, 13.
7. Klapperich, C.; Pruitt, L.; Komvopoulos, K. J Mater Sci: Mater Med 2001, 12, 549.
8. Li, R.; Ye, L.; Mai, Y. Compos A 1997, 28, 73.
9. Moon, S.; Jang, J. J Mat Sci 1998, 33, 3419.
10. Tressaud, A.; Durand, E.; Labrugere, C.; Kharitonov, A. P.; Kharitonova, L. N. J Fluorine Chem 2007, 128, 378.
11. Barni, R.; Riccardi, C.; Selli, E.; Massafra, M. R.; Marcandalli, B.; Orsini, F.; Poletti, G.; Meda, L. Plasma Proc Polym 2005, 2, 64.
12. Leonhardt, D.; Muratore, C.; Walton, S. G.; Meger, R. A. Surf Coat Technol 2004, 188, 299.
13. Leonhardt, D.; Walton, S. G.; Fernsler, R. F. Phys Plasmas 2007, 14, 057103.
14. Walton, S. G.; Muratore, C.; Leonhardt, D.; Fernsler, R. F.; Blackwell, D. D.; Meger, R. A. Surf Coat Technol 2004, 186, 40.
15. Manheimer, W. M.; Fernsler, R. F.; Lampe, M.; Meger, R. A. Plasma Sources Sci Technol 2000, 9, 370.
16. Lock, E. H.; Fernsler, R. F.; Walton, S. G. Plasma Sources Sci Technol 2008, 17, 025009.
17. Orf, B. J.; Walton, S. G.; Leonhardt, D.; Oehrlein, G. S. J Vac Sci Technol A 2007, 25, 779.
18. Lock, E. H.; Walton, S. G.; Fernsler, R. F. Plasma Proc Polym 2009, 6, 234.
19. Englemann, S.; Bruce, R. L.; Kwon, T.; Phaneuf, R.; Oehrlein, G. S.; Bae, Y. C.; Andes, C.; Graves, D.; Nest, D.; Hudson, E. A.; Lazzeri, P.; Lacob, E.; Anderle, M. J Vac Sci Technol B 2007, 25, 1353.
20. Walton, S. G.; Lock, E. H.; Fernsler, R. F. Plasma Proc Polym 2008, 5, 453.
21. Pappas, D. D.; Bujanda, A. A.; Orlicki, J. A.; Jensen, R. E. Surf Coat Technol 2008, 203, 830.
22. Leonhardt, D.; Walton, S. G.; Muratore, C.; Fernsler, F.; Meger, R. A. J Vac Sci Technol A 2004, 22, 2276.
23. Walton, S. G.; Green, J. E. Handbook of Thin Film Deposition Technology, 3rd Ed.; Peter Martin, Elsevier: Amsterdam, 2010.
24. Owens, D. K.; Wendt, R. C. J Appl Polym Sci 1969, 13, 1741.
25. Egitto, F. D.; Matienzo, L. Y.; Schneyer, H. B. J Vac Sci Technol 1992, 10, 3060.
26. Chenga, T.; Lina, H.; Chuang, M. Mater Lett 2004, 58, 650.
27. Lamperti, A.; Bottani, C. E.; Ossi, P. M. J Am Soc Mass Spectrom 2005, 16, 126.
28. Clain, S. R.; Egitto, F. D.; Emmi, F. J Vac Sci Technol 1987, 5, 1578.
29. Haidopoulos, M.; Horgnies, M.; Mirabella, F.; Pireaux, J. Plasma Process Polym 2008, 5, 67.
30. Zekonyte, J.; Zaporojtchenko, V.; Faupel, F. Nucl Instrum Methods Phys Res B 2005, 236, 241.
31. Hansen, R.; Schonhorn, H. Polym Lett 1966, 4, 203.
32. Pappas, D. D.; Bujanda, A.; Demaree, J. D.; Hirvonen, J. K.; Kosik, W.; Jensen, R.; Mcknight, S. Surf Coat Technol 2006, 201, 4384.
33. Corbin, G. A.; Cohen, R. E.; Baddour, R. F. Macromolecules 1985, 18, 98.
34. Friedrich, J. F.; Wigan, L.; Unger, W.; Lippitz, A.; Erdmann, J.; Gorsler, H.; Prescher, D.; Wittrich, H. Surf Coat Technol 1995, 74, 910.